

Black hole-neutron star mergers from triples II: the role of metallicity and spin-orbit misalignment

Giacomo Fragione^{1,2*}, Abraham Loeb³

¹*Department of Physics & Astronomy, Northwestern University, Evanston, IL 60202, USA*

²*Center for Interdisciplinary Exploration & Research in Astrophysics (CIERA), Evanston, IL 60202, USA*

³*Astronomy Department, Harvard University, 60 Garden St., Cambridge, MA 02138, USA*

16 October 2019

ABSTRACT

Observations of black hole-neutron star (BH-NS) mergers via gravitational waves (GWs) are of great interest for their electromagnetic counterparts, such as short gamma-ray bursts, and could provide crucial information on the nature of BHs and the NS crust and magnetosphere. While no event has been confirmed, a recent possible detection of a BH-NS merger event by the LIGO-Virgo collaboration has attracted a lot of attention to these sources. In this second paper of the series, we follow-up our study of the dynamical evolution of triples comprised of an inner BH-NS binary. In particular, we examine how the progenitor metallicity affects the characteristics of the BH-NS mergers in triples. We determine the distributions of masses, orbital parameters and merger times, as a function of the progenitor metallicity and initial triple orbital distributions, and show that the typical eccentricity in the LIGO band is $\sim 10^{-2} - 10^{-1}$. We derive a merger rate range of $\Gamma_{\text{BH-NS}} = 1.9 \times 10^{-4} - 22 \text{ Gpc}^{-3} \text{ yr}^{-1}$, consistent the LIGO-Virgo upper limit. Finally, we study the expected spin-orbit misalignments of merging BH-NS binaries from this channel, and find that typically the effective spin distribution is peaked at $\chi_{\text{eff}} \sim 0$ with significant tails.

Key words: galaxies: kinematics and dynamics – stars: black holes – stars: neutron – stars: kinematics and dynamics – Galaxy: kinematics and dynamics

1 INTRODUCTION

Several different astrophysical mechanisms have been proposed to explain the black hole (BH) and neutron star (NS) binary mergers observed via gravitational wave (GW) emission by the LIGO-Virgo collaboration. Scenarios include isolated binary evolution (Belczynski et al. 2016; de Mink & Mandel 2016; Kruckow et al. 2018; Eldridge et al. 2019), mergers in star clusters (Askar et al. 2017; Banerjee 2018; Fragione & Kocsis 2018; Rodriguez et al. 2018), GW capture events and Kozai-Lidov (KL) mergers in galactic nuclei (O’Leary et al. 2009; Antonini & Perets 2012; Fragione et al. 2018; Grishin et al. 2018; Rasskazov & Kocsis 2019), mergers in active galactic nuclei accretion disks (Bartos et al. 2017), and KL mergers in isolated triple and quadruple systems (Antonini et al. 2017; Silsbee & Tremaine 2017; Arca-Sedda et al. 2018; Fragione & Kocsis 2019; Liu & Lai 2019).

LIGO-Virgo promise to observe a large number of BH-BH, BH-NS and NS-NS mergers in the next few years and to shed light on their origin. Thus, it is of crucial importance to examine the different contributions to the overall observed

rate. It has been shown that the distributions of masses, spins, eccentricity and redshift of the merging compact objects could be used to statistically disentangle the contributions of different origins (see e.g. O’Leary et al. 2016; Gondán et al. 2018). For example, BHs and NSs merging in triples and quadruples are expected to retain significant eccentricities when entering the LIGO band (10 Hz), much larger than binaries that merge in isolation (see e.g. Antonini et al. 2016; Fragione et al. 2018; Fragione & Bromberg 2019).

The O2 catalogue of compact object mergers released by the LIGO-Virgo collaboration includes ten BH binaries and one NS binary (The LIGO Scientific Collaboration & the Virgo Collaboration 2018). No BH-NS mergers have been observed, even though there are now possible candidate events amongst GW detections (see e.g. LVC GCN 24237 and LVC GCN 25324). BH-NS mergers might have electromagnetic (EM) counterparts, such as short gamma-ray bursts, which can provide crucial information on the related accretion onto stellar BHs and provide unique information on the NS crust and magnetosphere (Pannarale et al. 2011; Foucart 2012; Tsang et al. 2012; D’Orazio & Levin 2013).

The origin of BH-NS mergers is still highly uncertain

* E-mail: giacomo.fragione@northwestern.edu

Table 1. Description of important quantities used in the text.

Symbol	Description
m_{BH}	Mass of the black hole in the inner binary
m_{NS}	Mass of the neutron star in the inner binary
m_3	Mass of the third companion in the triple
a_{in}	Semi-major axis of the inner (black hole-neutron star) orbit
e_{in}	Eccentricity of the inner (black hole-neutron star) orbit
a_{out}	Semi-major axis of the outer orbit
e_{out}	Eccentricity of the outer orbit
i_0	Inclination between the inner and outer orbits
$a_{3,\text{max}}$	Maximum outer semi-major axis of the triple
σ_{BH}	Dispersion of black hole kick-velocity distribution
σ_{NS}	Dispersion of neutron star kick-velocity distribution
Z	Progenitor metallicity
χ_{BH}	Kerr parameter of the black hole
χ_{NS}	Kerr parameter of the neutron star

and debated. BH-NS binaries can be produced in isolation as a result of binary evolution, as for BH-BH and NS-NS binaries (de Mink & Mandel 2016; Kruckow et al. 2018; Eldridge et al. 2019). More complicated is the process of forming BH-NS binaries through dynamical assembly in star clusters. A number of papers showed that NSs are generally prevented from forming NS-NS and BH-NS binaries in a star cluster as a result of the strong heating due to gravitational BH scatterings (Fragione et al. 2018; Ye et al. 2019). Only if most of the BHs have been ejected from the cluster, NSs can efficiently segregate in the innermost regions and possibly form binaries, that later merge. Recently, Fragione & Loeb (2019) have proposed that BH-NS mergers can be a natural outcome of the dynamical evolution of triple systems. Here, the KL cycles imposed by the tidal field of the tertiary can make the inner BH-NS binary reach high eccentricities and merge as a consequence of the efficient dissipation of energy through GW emission at pericentre.

In this second paper of the series, we follow-up our study of the dynamical evolution of triples comprised of an inner BH-NS binary (Fragione & Loeb 2019), by means of high-precision N -body simulations, including Post-Newtonian (PN) terms up to 2.5PN. We start from the main sequence progenitors of the BHs and model the supernova (SN) events that lead to the formation of the BH triple. We adopt different prescriptions for SN natal kicks and orbital parameters. We also take into account different progenitor metallicities to study how this parameter affects the characteristics of the BH-NS mergers in triples. We determine the distributions of various merger properties, including masses, eccentricities, and merger times. Finally, we also investigate the expected spin-orbit misalignments of merging BH-NS binaries from this channel.

The paper is organized as follows. In Section 2, we discuss the initial conditions adopted in this paper. In Section 3, we discuss the parameters of merging systems and present the distributions of masses, eccentricities and spin-orbit misalignments. Finally, in Section 4, we discuss the implications of our findings and summarize our conclusions.

2 METHOD

First, we describe our initial population of stellar triples. In total, we consider eight different models (see Table 2).

We consider a triple system that consists of an inner binary of mass $m_{\text{in}} = m_1 + m_2$ ($m_1 > m_2$) and a third body of mass m_3 that orbits the inner binary. The semi-major axis and eccentricity of the inner orbit are a_{in} and e_{in} , respectively, while the semi-major axis and eccentricity of the outer orbit are a_{out} and e_{out} , respectively. The inner and outer orbital plane have initial mutual inclination i_0 .

In all our models, we sample the mass m_1 from a canonical initial mass function (Kroupa 2001),

$$\frac{dN}{dm} \propto m^{-2.3}, \quad (1)$$

in the mass range $20 M_{\odot}$ - $150 M_{\odot}$, reflecting the progenitor of the BH. We adopt a flat mass ratio distribution for both the inner binary, m_2/m_1 , and the outer binary, $m_3/(m_1 + m_2)$ (Sana et al. 2012; Duchêne & Kraus 2013; Sana 2017). We sample the mass of the secondary in the inner binary in the mass range $8 M_{\odot}$ - $20 M_{\odot}$, reflecting the progenitor of the NS. The mass third star is sampled in the range $0.5 M_{\odot}$ - $150 M_{\odot}$ ¹.

We sample the distribution of the inner and outer semi-major axis, a_{in} and a_{out} , respectively, from a log-uniform (Kobulnicky et al. 2014). We set a minimum inner separation of 10 AU (Fragione & Loeb 2019), while we adopt two different values for the maximum separation of the triple, $a_{3,\text{max}} = 2000 \text{ AU}$ - 5000 AU (Sana et al. 2014). We then assume a flat distribution for the orbital eccentricities of the inner binary, e_{in} , and outer binary, e_{out} (Antonini et al. 2017). Finally, the initial mutual inclination i_0 between the inner and outer orbits is drawn from an isotropic distribution, while the other relevant angles are drawn randomly.

After sampling the relevant parameters, we check that the initial configuration satisfies the stability criterion of hierarchical triples of Mardling & Aarseth (2001). Otherwise, we sample the triple parameters again according to the above procedure.

We assume that the stars in the inner binary undergo a

¹ We are not taking into account a possible dependence of the IMF on the metallicity (Marks et al. 2012)

Table 2. Models parameters: name, dispersion of BH kick-velocity distribution (σ_{BH}), dispersion of the NS kick-velocity distribution (σ_{NS}), progenitor metallicity (Z), maximum outer semi-major axis of the triple ($a_{3,\text{max}}$), fraction of stable triple systems after SNe (f_{stable}), fraction of stable systems that merge from the N -body simulations (f_{merge}).

Name	σ_{BH} (km s $^{-1}$)	σ_{NS} (km s $^{-1}$)	Z	$a_{3,\text{max}}$ (AU)	f_{stable}	f_{merge}
A1	$\sigma_{\text{NS}} \times (m_{\text{NS}}/m_{\text{BH}})$	260	0.01	2000	2.6×10^{-7}	0.13
A2	$\sigma_{\text{NS}} \times (m_{\text{NS}}/m_{\text{BH}})$	100	0.01	2000	1.8×10^{-5}	0.11
A3	$\sigma_{\text{NS}} \times (m_{\text{NS}}/m_{\text{BH}})$	0	0.01	2000	1.4×10^{-2}	0.13
B1	$\sigma_{\text{NS}} \times (m_{\text{NS}}/m_{\text{BH}})$	260	0.0001	2000	5.5×10^{-4}	0.10
B2	$\sigma_{\text{NS}} \times (m_{\text{NS}}/m_{\text{BH}})$	260	0.001	2000	1.4×10^{-4}	0.07
B3	$\sigma_{\text{NS}} \times (m_{\text{NS}}/m_{\text{BH}})$	260	0.005	2000	1.6×10^{-6}	0.11
B4	$\sigma_{\text{NS}} \times (m_{\text{NS}}/m_{\text{BH}})$	260	0.015	2000	5.1×10^{-8}	0.12
C1	$\sigma_{\text{NS}} \times (m_{\text{NS}}/m_{\text{BH}})$	260	0.01	5000	1.4×10^{-7}	0.11

SN event sequentially. We also assume that every SN takes place instantaneously, that is on a time-scale shorter than the orbital period, during which the exploding star has an instantaneous removal of mass and is converted to a BH (m_1) or a NS (m_2) (Pijloo et al. 2012; Toonen et al. 2016; Fragione & Loeb 2019). We determine the final mass m_{BH} of the BH by using the fitting formulae to the results of the PARSEC stellar evolution code (see Appendix C in Spera et al. 2015). We adopt five different values of the metallicity, $Z = 0.0001-0.001-0.005-0.01-0.015$, which ultimately set the final mass of the BH remnant². The final mass of the secondary, which produces a NS, is set to $m_{\text{NS}} = 1.3 M_{\odot}$.

As a result of the mass loss, the exploding star is imparted a kick to its center of mass (Blaauw 1961). Furthermore, the system receives a natal kick due to recoil from an asymmetric supernova explosion. We assume that the natal velocity kick is drawn from a Maxwellian distribution,

$$p(v_k) \propto v_k^2 e^{-v_k^2/\sigma^2}, \quad (2)$$

with a mean velocity σ . The value of σ is highly uncertain. We implement momentum-conserving kicks, i.e. we assume that the momentum imparted to a BH is the same as the momentum given to a NS (Fryer & Kalogera 2001). Therefore, the natal kick velocity for the BHs is simply $\sigma_{\text{BH}} = \sigma_{\text{NS}} \times (1.3 M_{\odot}/m_{\text{BH}}) = \sigma \times (1.3 M_{\odot}/m_{\text{BH}})$. In our fiducial model, we consider $\sigma = 260 \text{ km s}^{-1}$ (Hobbs et al. 2005). Additionally, we run a model where we set $\sigma = 100 \text{ km s}^{-1}$ (Arzoumanian et al. 2002), and also adopt a model where no natal kick (i.e. $\sigma = 0 \text{ km s}^{-1}$) is imparted during BH and NS formation. For NSs, this could reflect the formation process of electron-capture SN (Podsiadlowski et al. 2004). In the case $m_3 \geq 8 M_{\odot}$, we let it undergo an SN event and conversion to a compact object as well. In the case it collapses to a BH, the final mass m_3^{fin} is computed using the same formulae used for the primary star, while $m_3^{\text{fin}} = 1.3 M_{\odot}$ in the case it produces a NS. If $m_3 < 8 M_{\odot}$, then $m_3^{\text{fin}} = m_3$.

After each SN event, the orbital elements of the triple are updated as appropriate (see e.g. Fragione & Loeb 2019), to account both for mass loss and natal kicks (Blaauw 1961).

We also check again that the stability criterion of hierarchical triples of Mardling & Aarseth (2001) is satisfied and the triple is stable. After all the SNe take place, we integrate the triple systems by means of the ARCHAIN code (Mikkola & Merritt 2006, 2008), a fully regularized code able to model the evolution of binaries of arbitrary mass ratios and eccentricities with high accuracy and that includes PN corrections up to order PN2.5. We performed $\sim 700-1000$ simulations for each model in Table 2. We fix the maximum integration time as (Sillsbee & Tremaine 2017; Fragione & Loeb 2019),

$$T = \min(10^3 \times T_{\text{KL}}, 10 \text{ Gyr}), \quad (3)$$

where T_{KL} is the triple KL timescales,

$$T_{\text{KL}} = \frac{8}{15\pi} \frac{m_{\text{tot}}}{m_3^{\text{fin}}} \frac{P_{\text{out}}^2}{P_{\text{in}}} (1 - e_{\text{out}}^2)^{3/2}. \quad (4)$$

Here, $m_{\text{tot}} = m_{\text{BH}} + m_{\text{NS}} + m_3^{\text{fin}}$ and P_{in} and P_{out} are the inner and outer orbital period, respectively. In the case the third companion does not collapse to a compact object, i.e. $m_3 < 8 M_{\odot}$, we set as the maximum timescale the minimum between Eq. 3 and its MS lifetime, which is simply parametrised as (e.g. Iben 1991; Hurley et al. 2000; Maeder 2009),

$$\tau_{\text{MS}} = \max(10 (m/M_{\odot})^{-2.5} \text{ Gyr}, 7 \text{ Myr}). \quad (5)$$

In this case, we also check if the third star overflows its Roche lobe (Eggleton 1983). In such a case, we stop the integration³.

3 RESULTS

Next, we discuss the parameters of merging BH-NS systems and present the distributions of masses, eccentricities and spin-orbit misalignments. Finally, we also compute the typical merger rate of BH-NS systems in triples.

3.1 Inner and outer semi-major axis

Figure 1 reports the cumulative distribution function (CDF) of inner (top) and outer (bottom) semi-major axis of BH-NS

² We ignore the SN-shell impact on the companion stars. We are not modelling the mass loss during neither possible episodes of Roche-lobe overflows nor possible common evolution phases. Both these processes are not well understood and modeled in triple systems. For recent discussion see Di Stefano (2019) and Hamers & Dosopoulou (2019).

³ We do not model the process that leads to the formation of a white dwarf for the third companion. If the tertiary becomes a white dwarf and the system remains bound, some of the systems could still merge via KL oscillations.

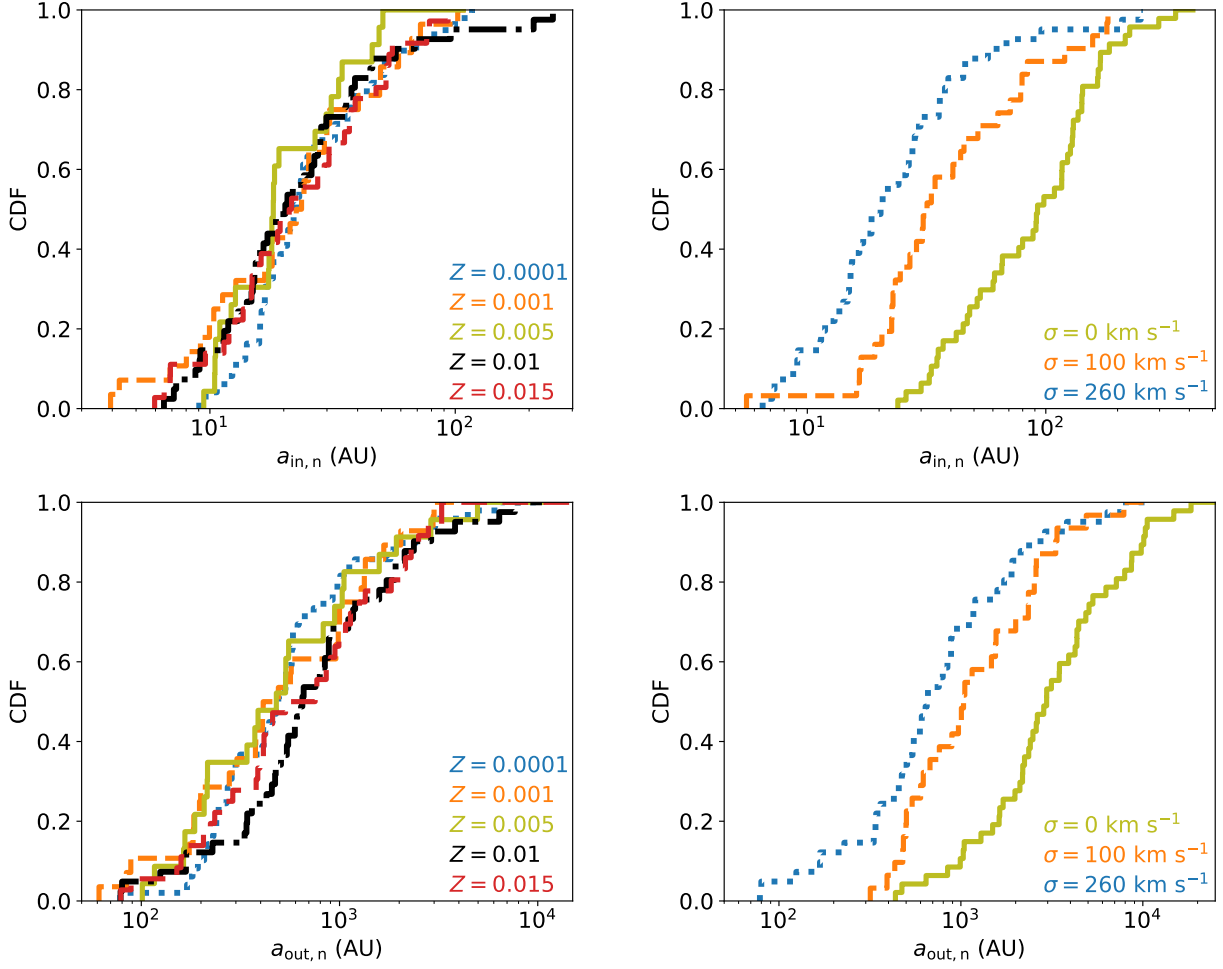


Figure 1. Cumulative distribution function of inner (top) and outer (bottom) semi-major axis of BH-NS binaries in triples that lead to a merger. Left panel: a_{in} and a_{out} for different progenitor metallicities Z ($\sigma = 260 \text{ km s}^{-1}$ and $a_{3,\text{max}} = 2000 \text{ AU}$); right panel: a_{in} and a_{out} for different values of σ ($Z = 0.01$ and $a_{3,\text{max}} = 2000 \text{ AU}$).

binaries in triples that lead to a merger. In the left panel, we show the distribution of a_{in} and a_{out} for different values of the metallicity Z ($\sigma = 260 \text{ km s}^{-1}$ and $a_{3,\text{max}} = 2000 \text{ AU}$). We find that the metallicity does not affect the distribution of the inner and outer semi-major axes. In right panel, we show the CDFs of a_{in} and a_{out} for different values of σ , for Models A1-A2-A3. In these models, $Z = 0.01$ and $a_{3,\text{max}} = 2000 \text{ AU}$. As shown in Fragione & Loeb (2019), the value of the mean natal velocity kick of Eq. 2 affects the distribution of the semi-major axes of the triples that lead to a BH-NS merger. We find that $\sim 50\%$ of the systems have $a_{\text{in}} \lesssim 100 \text{ AU}$, $\lesssim 30 \text{ AU}$, $\lesssim 20 \text{ AU}$ for $\sigma = 0 \text{ km s}^{-1}$, 100 km s^{-1} , 260 km s^{-1} , respectively, and $\sim 50\%$ of the systems have $a_{\text{out}} \lesssim 3000 \text{ AU}$, $\lesssim 1000 \text{ AU}$, $\lesssim 700 \text{ AU}$ for $\sigma = 0 \text{ km s}^{-1}$, 100 km s^{-1} , 260 km s^{-1} , respectively.

3.2 Mass distribution

The typical values of Z and σ are expected to have an impact on the distribution of BH masses. Lower metallicity progenitors collapse to make heavier BHs. For $Z \gtrsim 0.002$, the final BH mass is limited to $\sim 60 M_{\odot}$, while for smaller metallicities the progenitor can even collapse to make a BH of mass

$\sim 120 M_{\odot}$ – $140 M_{\odot}$ (Spera et al. 2015). The effect of σ on the BH mass distribution can be understood in terms of our assumption of momentum-conserving kicks, where higher mass BHs receive lower velocity kicks, since $\sigma_{\text{BH}} \propto m_{\text{BH}}^{-1}$. Therefore, more massive BHs, which are preferentially produced from low-metallicity progenitors, are more likely to be retained in triples and eventually merge with the NS.

We illustrate how the CDF of m_{BH} of BH-NS binaries in triples that lead to a merger depends on the progenitor metallicity in the top panel of Figure 2, for $\sigma = 260 \text{ km s}^{-1}$ and $a_{3,\text{max}} = 2000 \text{ AU}$. For $Z \gtrsim 0.005$, we find that the distribution of BH masses is not significantly affected by value of the progenitor metallicity. For these values of Z , we find that most of the mergers have $m_{\text{BH}} \lesssim 40 M_{\odot}$. On the other hand, m_{BH} is in the range $\sim 40 M_{\odot}$ – $80 M_{\odot}$ and $\sim 60 M_{\odot}$ – $130 M_{\odot}$ for $Z = 0.001$ and $Z = 0.0001$, respectively.

In the bottom panel of Figure 2, we illustrate how the CDF of m_{BH} of BH-NS binaries in triples that lead to a merger depends on the mean natal kick, for $Z = 0.01$ and $a_{3,\text{max}} = 2000 \text{ AU}$. In the case of $\sigma = 0 \text{ km s}^{-1}$, we find that $\sim 50\%$ of the BHs that merge have mass $\lesssim 18 M_{\odot}$, while \sim

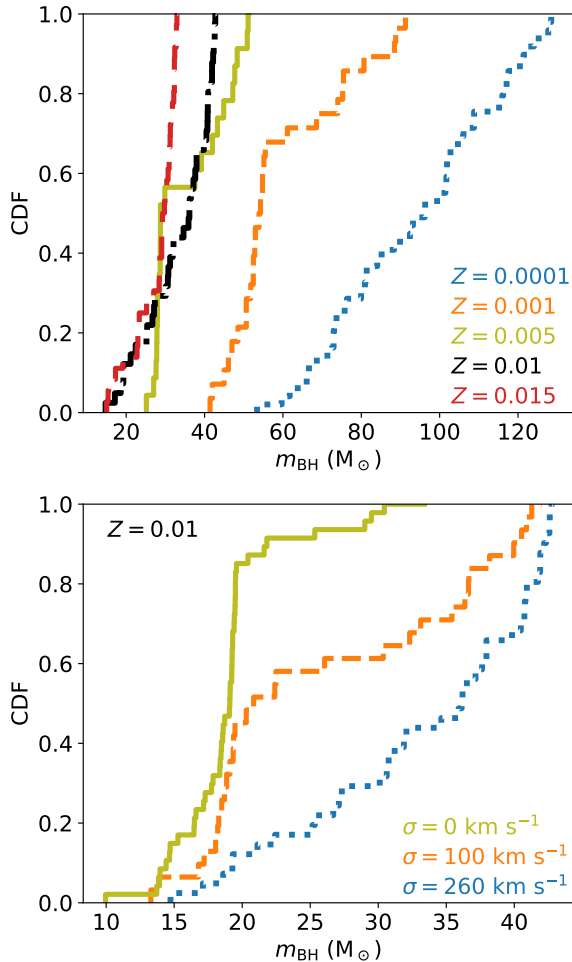


Figure 2. Cumulative distribution function of the BH mass of BH-NS binaries in triples that lead to a merger, for different values of Z (top) and σ (bottom).

50% of the BHs that merge have mass $\lesssim 22 M_{\odot}$ and $\lesssim 37 M_{\odot}$ for $\sigma = 100 \text{ km s}^{-1}$ and $\sigma = 260 \text{ km s}^{-1}$, respectively⁴.

Figure 3 shows the cumulative distribution function of the chirp mass,

$$m_{\text{chirp}} = \frac{(m_{\text{BH}} m_{\text{NS}})^{3/5}}{(m_{\text{BH}} + m_{\text{NS}})^{1/5}} \quad (6)$$

of BH-NS binaries in triples that lead to a merger, for different values of Z (top) and σ (bottom). As before, lower progenitor metallicities predict higher values of m_{chirp} . For $Z \gtrsim 0.005$, the distribution of chirp masses is not significantly affected by Z , and most of the mergers have $m_{\text{chirp}} \lesssim 5 M_{\odot}$, while m_{chirp} is in the range $\sim 5 M_{\odot} - 7 M_{\odot}$ and $\sim 6 M_{\odot} - 8 M_{\odot}$ for $Z = 0.001$ and $Z = 0.0001$, respectively. Higher natal kicks prefer higher values of m_{chirp} .

3.3 Eccentricity

Hierarchical configurations are expected to have eccentricities when entering the LIGO band (10 Hz) that are larger

⁴ Other models for the kicks may lead to different mass distributions.

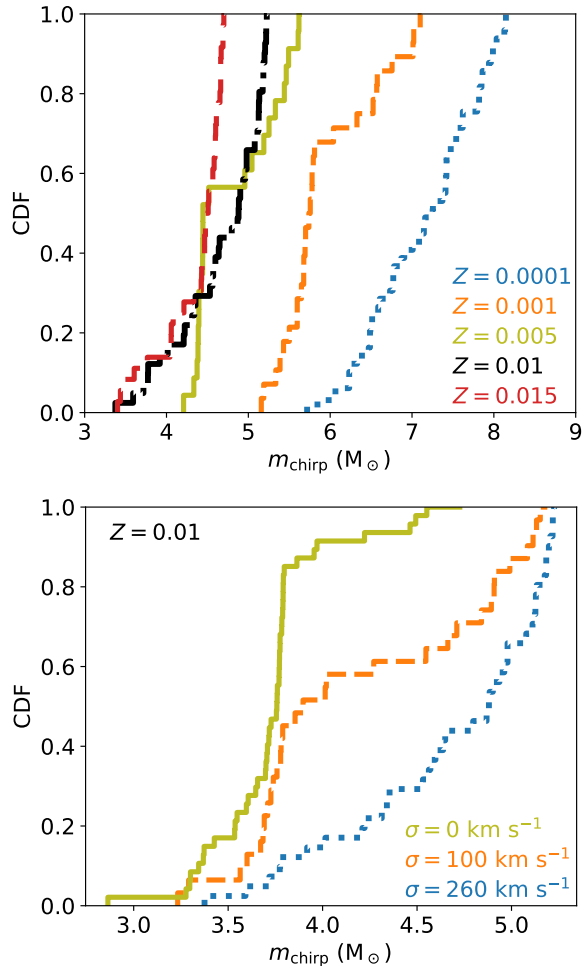


Figure 3. Cumulative distribution function of the chirp mass of BH-NS binaries in triples that lead to a merger, for different values of Z (top) and σ (bottom).

than for binaries that merge in isolation (see e.g. Antonini et al. 2016; Fragione et al. 2018; Fragione & Bromberg 2019). For the BH binaries that merge in our simulations, we compute a proxy for the GW frequency, i.e. the frequency corresponding to the harmonic that gives the maximum GW emission (Wen 2003),

$$f_{\text{GW}} = \frac{\sqrt{G(m_{\text{BH}} + m_{\text{NS}})}}{\pi} \frac{(1 + e_{\text{in}})^{1.1954}}{[a_{\text{in}}(1 - e_{\text{in}}^2)]^{1.5}}. \quad (7)$$

Figure 4 illustrates the distribution (PDF) of eccentricities at the moment the BH binaries enter the LIGO frequency band. We also plot the minimum $e_{10\text{Hz}} = 0.081$ where LIGO could start distinguishing eccentric sources from circular sources (Gondán & Kocsis 2019). A large fraction of systems that merge have a significant eccentricity in the LIGO band, compared to binaries that merge in isolation. We note that a similar signature could be found in BH binaries that merge near supermassive black holes (Fragione et al. 2018, 2019), in the BH-BH binaries that merge in star clusters (Samsing et al. 2014a; Samsing 2018; Samsing et al. 2019), and in isolated hierarchical triples (Antonini et al. 2017) and quadruples (Fragione & Kocsis 2019).

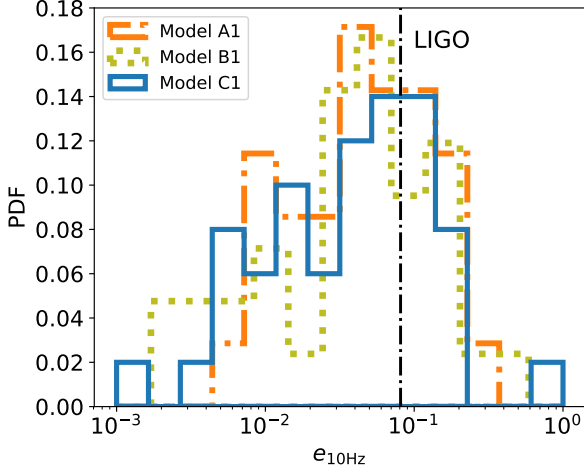


Figure 4. Distribution of eccentricities at the moment the BH-NS binaries enter the LIGO frequency band (10 Hz). The vertical line reports the minimum eccentricity ($e_{10\text{Hz}} = 0.081$) where LIGO may start distinguishing eccentric sources from circular sources (Gondán & Kocsis 2019).

3.4 Effective spin

We describe the BH and NS spins with their respective spin vectors $\mathbf{S}_{\text{BH}} = S_{\text{BH}}\hat{\mathbf{S}}_{\text{BH}}$ and $\mathbf{S}_{\text{NS}} = S_{\text{NS}}\hat{\mathbf{S}}_{\text{NS}}$, where $S_{\text{BH}} = (Gm_{\text{BH}}^2/c)\chi_{\text{BH}}$ and where $S_{\text{NS}} = (Gm_{\text{NS}}^2/c)\chi_{\text{NS}}$. In the previous equations, $0 \leq \chi_{\text{BH}} \leq 1$ and $0 \leq \chi_{\text{NS}} \leq 1$ are the Kerr parameter of the BH and NS, respectively. Rather than the single spins of the two merging objects, GW measurements are sensible to a combination of them,

$$\chi_{\text{eff}} = \frac{m_{\text{BH}}\chi_{\text{BH}} \cos\theta_{\text{BH}} + m_{\text{NS}}\chi_{\text{NS}} \cos\theta_{\text{NS}}}{m_{\text{BH}} + m_{\text{NS}}}, \quad (8)$$

where $\cos\theta_{\text{BH}} = (\hat{\mathbf{S}}_{\text{BH}} \cdot \mathbf{J})/J$ and $\cos\theta_{\text{NS}} = (\hat{\mathbf{S}}_{\text{NS}} \cdot \mathbf{J})/J$, where \mathbf{J} is the BH-NS orbital angular momentum.

The spins of the BHs and NSs in the inner binary can undergo a relativistic precession around \mathbf{J} , as a consequence of the KL cycles. In our simulations, we model the spin-orbit coupling as in Liu et al. (2019). The De Sitter geodetic precession of the spins \mathbf{S}_{BH} and \mathbf{S}_{NS} of the BHs in the inner binary around the inner binary angular momentum \mathbf{J} is given by,

$$\frac{d\mathbf{S}_{\text{BH}}}{dt} = \boldsymbol{\Omega}_{\text{BH}} \times \mathbf{S}_{\text{BH}} = \left[\frac{2G\mu}{c^2 r^3} \left(1 + \frac{3m_{\text{NS}}}{4m_{\text{BH}}} \right) \mathbf{r} \times \mathbf{v} \right] \times \mathbf{S}_{\text{BH}} \quad (9)$$

$$\frac{d\mathbf{S}_{\text{NS}}}{dt} = \boldsymbol{\Omega}_{\text{NS}} \times \mathbf{S}_{\text{NS}} = \left[\frac{2G\mu}{c^2 r^3} \left(1 + \frac{3m_{\text{BH}}}{4m_{\text{NS}}} \right) \mathbf{r} \times \mathbf{v} \right] \times \mathbf{S}_{\text{NS}}, \quad (10)$$

where μ is the inner binary reduced mass, $\mathbf{r} = \mathbf{r}_{\text{BH}} - \mathbf{r}_{\text{NS}}$ and $\mathbf{v} = \mathbf{v}_{\text{BH}} - \mathbf{v}_{\text{NS}}$ ⁵.

We take seven different models for the spins, which differ for the initial magnitude of the Kerr parameters and/or the initial orientation of the spins (see Table 3)

- Model S1: χ_{BH} and χ_{NS} are drawn independently from an uniform distribution and the initial misalignments of the

Table 3. Spin models: name, Kerr parameter of the BH (χ_{BH}), Kerr parameter of the NS (χ_{NS}), initial misalignment of the BH spin ($\cos\theta_{\text{BH}}^{\text{ini}}$) and NS spin ($\cos\theta_{\text{NS}}^{\text{ini}}$) with respect to \mathbf{J} .

Name	χ_{BH}	χ_{NS}	Initial misalignment
S1	uniform	uniform	$0^\circ \leq \cos\theta_{\text{BH,NS}}^{\text{ini}} \leq 20^\circ$
S2	Eq. 11	uniform	$0^\circ \leq \cos\theta_{\text{BH,NS}}^{\text{ini}} \leq 20^\circ$
T1	uniform	uniform	aligned to \mathbf{J}
T2	uniform	uniform	isotropic
U1	0.2	0.2	$0^\circ \leq \cos\theta_{\text{BH,NS}}^{\text{ini}} \leq 20^\circ$
U2	0.5	0.5	$0^\circ \leq \cos\theta_{\text{BH,NS}}^{\text{ini}} \leq 20^\circ$
U3	0.8	0.8	$0^\circ \leq \cos\theta_{\text{BH,NS}}^{\text{ini}} \leq 20^\circ$

BH spin ($\cos\theta_{\text{BH}}^{\text{ini}}$) and NS spin ($\cos\theta_{\text{NS}}^{\text{ini}}$) with respect to \mathbf{J} are drawn uniformly in the range 0° – 20° ;

- Model S2: the dimensionless BH spin is set by the BH mass (Belczynski et al. 2017),

$$\chi = \frac{p_1 - p_2}{2} \tanh\left(p_3 - \frac{m_{\text{BH}}}{M_\odot}\right) + \frac{p_1 + p_2}{2}, \quad (11)$$

where $p_1 = 0.86 \pm 0.06$, $p_2 = 0.13 \pm 0.13$, and $p_3 = 29.5 \pm 8.5$. Spins are then generated by drawing random samples uniformly in the region in between the two curves given by the upper and lower limits of the parameters (Gerosa et al. 2018). The dimensionless NS spin is drawn from an uniform distribution, while $0^\circ \leq \cos\theta_{\text{BH,NS}}^{\text{ini}} \leq 20^\circ$ uniformly;

- Model T1: χ_{BH} and χ_{NS} are drawn independently from an uniform distribution and the BH and NS spins are initially aligned to the BH-NS angular momentum;

- Model T2: χ_{BH} and χ_{NS} are drawn independently from an uniform distribution and the initial spin-orbit misalignments of BH and NS are drawn from an isotropic distribution;

- Models U1, U2, U3: the BH and NS Kerr parameters are fixed to 0.2–0.5–0.8, respectively, and $0^\circ \leq \cos\theta_{\text{BH,NS}}^{\text{ini}} \leq 20^\circ$ uniformly.

In Figure 5, we show the effective spin distributions of BH-NS binaries in triples that lead to merger for different values of Z (top: Model B1; centre: Model A1; bottom: Model B4) and all the spin models in Table 3. In Models S1-S2-T1-T2 (left panel), the χ_{eff} distribution is not affected by the initial choice of the BH and NS spins, for $Z = 0.01$ and $Z = 0.015$. The distributions have a peak at $\chi_{\text{eff}} \sim 0$ and broad tails up to ± 1 . We find a similar trend for all the spin models also for $Z = 0.0001$, except for the Model S2. In these model, we sample χ_{BH} according to Eq. 11, where more massive BHs have on average smaller initial spins. Moreover, for $Z = 0.0001$, the final mass of the BH (see Figure 2) may be considerably higher than the mass of the NS. As a result, χ_{eff} could be mainly determined by the BH contribution, and only slightly affected by the NS, thus result in a distribution peaked at $\chi_{\text{eff}} \sim 0$ and negligible tails.

In the spin models where we fix the BH and NS Kerr parameters (right panel), the final distributions of χ_{eff} do not depend substantially on the progenitor metallicity and present a similar behaviour for all Z 's. The distributions appear more broadly distributed over the possible values of χ_{eff} for larger initial Kerr parameters. As the initial spin magnitudes are decreased, the distributions converge to zero.

Figure 6 illustrates the distributions of χ_{eff} of BH-NS

⁵ We neglect the backreaction of \mathbf{S}_{BH} and \mathbf{S}_{NS} on \mathbf{J} and the spin-spin precessional terms (Antonini et al. 2018; Liu et al. 2019).

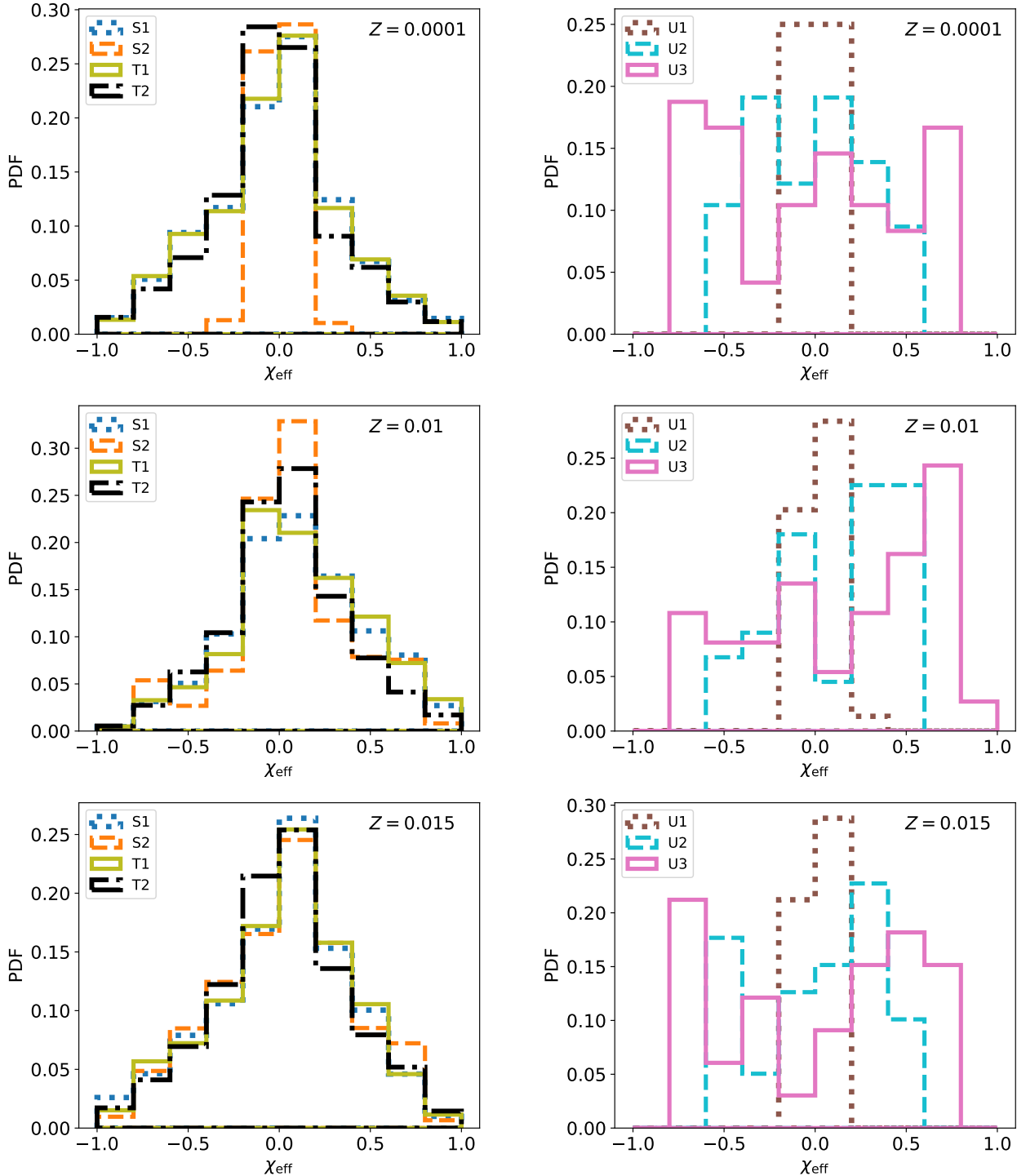


Figure 5. Effective spin distributions of BH-NS binaries in triples that lead to merger for different values of Z (top: Model B1; centre: Model A1; bottom: Model B4) and all the spin models under consideration (see Table 3).

binaries in triples that lead to merger for different values of σ (top: Model A3; centre: Model A2; bottom: Model A1) and all the spin models in Table 3. Also here, in Models S1-S2-T1-T2 (left panel), the χ_{eff} distribution is not affected by the initial choice of the BH and NS spins. The only exception is the χ_{eff} distribution for Model S2 in the case $\sigma = 0 \text{ km s}^{-1}$, where the distribution appears more flat. In

the models where we fix the BH and NS Kerr parameters (right panel), the final distributions of χ_{eff} do not depend substantially on σ and present a similar behaviour described above for different progenitor metallicities.

Finally, we find nearly no difference in the final distributions of the effective spin for Model C1, where we set $a_{3,\text{max}} = 5000 \text{ AU}$, compared to our fiducial Model A1.

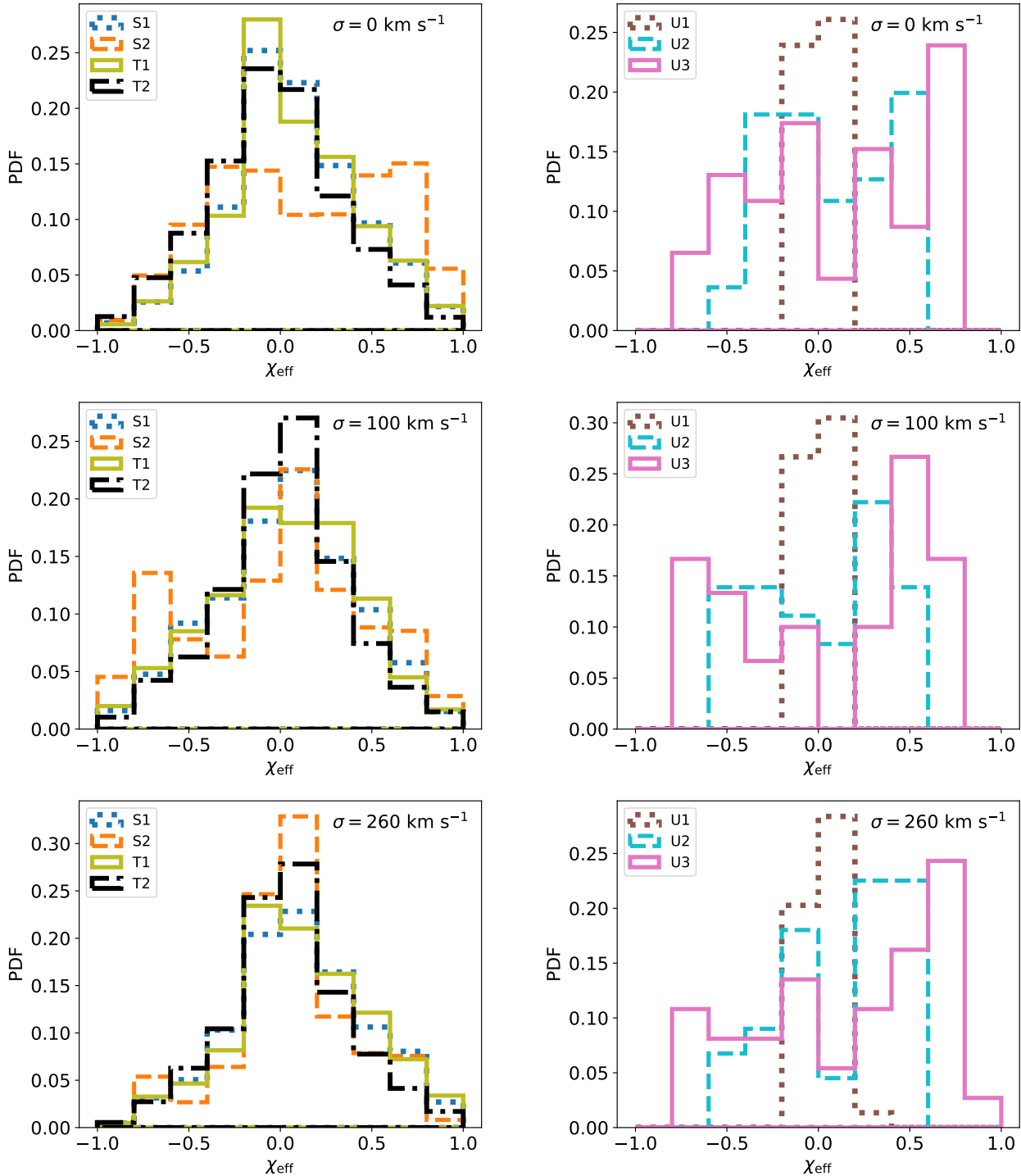


Figure 6. Effective spin distributions of BH-NS binaries in triples that lead to merger for different values of σ (top: Model A3; centre: Model A2; bottom: Model A1) and all the spin models under consideration (see Table 3).

We also show in Figure 7 the distributions of the absolute misalignment θ_{BH} between \mathbf{S}_{BH} and \mathbf{J} , θ_{NS} between \mathbf{S}_{NS} and \mathbf{J} , and the relative misalignment between \mathbf{S}_{BH} and \mathbf{S}_{NS} for Model A1 and the first four spin models of Table 3. We find that for the spin Models S1-S2-T1, the distributions are similar to each other, while differences arise for Model T2. In particular, the distribution of $|\theta_{\text{BH}} - \theta_{\text{NS}}|$ appears

broader than for the other models. This is a result of the fact that the initial misalignment of the BH and NS spins is drawn from an isotropic distribution.

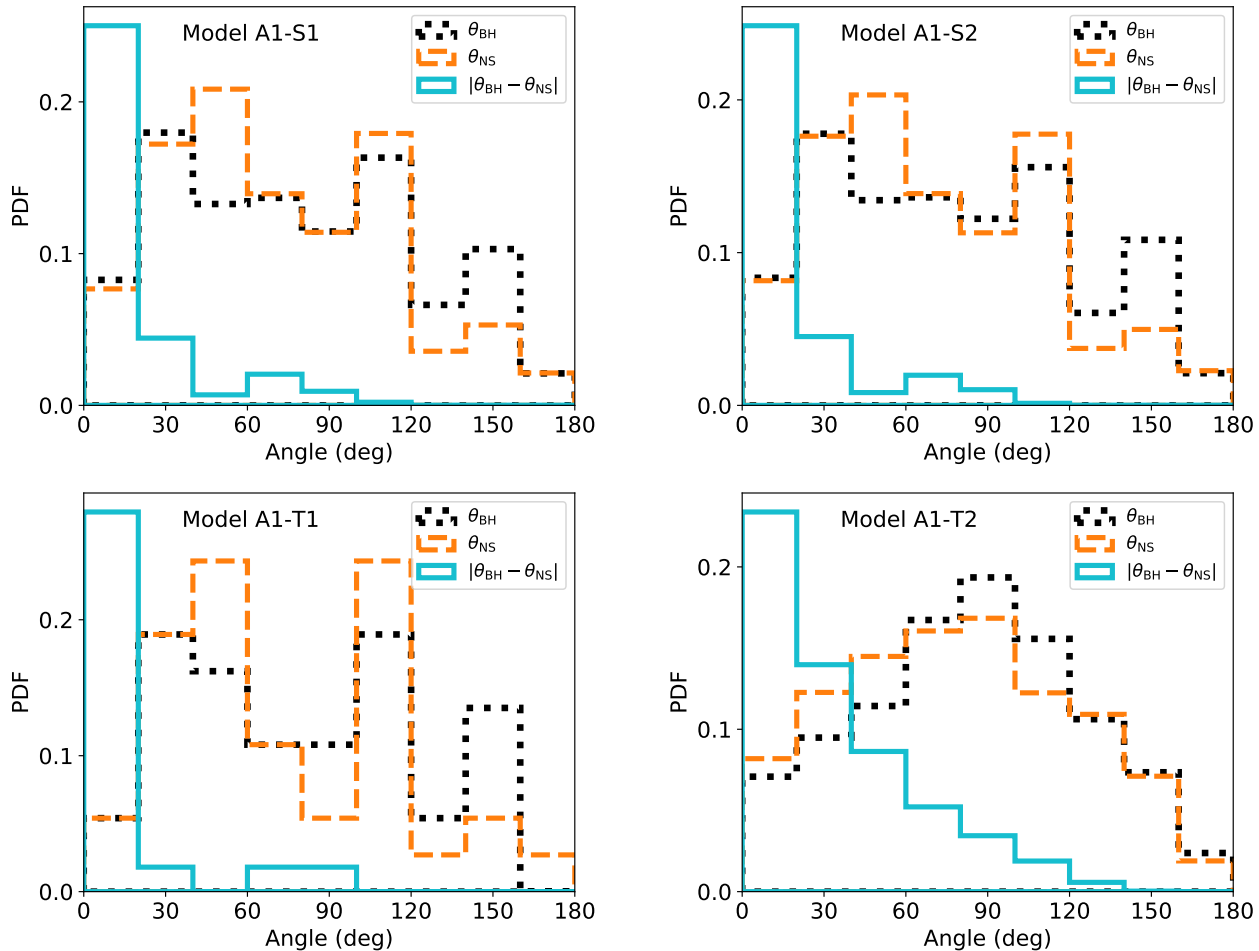


Figure 7. Distributions of the absolute misalignment θ_{BH} between \mathbf{S}_{BH} and \mathbf{J} , θ_{NS} between \mathbf{S}_{NS} and \mathbf{J} , and the relative misalignment between \mathbf{S}_{BH} and \mathbf{S}_{NS} for Model A1 and the first four spin models of Table 3.

3.5 Merger times

Figure 8 shows the merger time (after the SN events) CDFs of BH-NS binaries in triples that lead to merger for all models. The CDF does not depend significantly on Z , but depends mostly on σ . Larger kick velocities imply a larger outer semi-major axis, thus a larger typical KL timescale since $T \propto a_{\text{out},n}^3$. Compared to the case of $\sigma = 0 \text{ km s}^{-1}$, the typical merger time is 2–3 times longer when $\sigma = 260 \text{ km s}^{-1}$. Different $a_{3,\text{max}}$'s (Model C1) do not affect significantly the merger time distribution.

In order to compute the merger rate of BH-NS binaries, we follow the scheme adopted in Fragione & Loeb (2019). Assuming a local star formation rate of $0.025 M_{\odot} \text{ Mpc}^{-3} \text{ yr}^{-1}$, the number of stars formed per unit mass is given by (Bothwell et al. 2011),

$$N(m)dm = 5.4 \times 10^6 m^{-2.3} \text{ Gpc}^{-3} \text{ yr}^{-1}, \quad (12)$$

and assuming a constant star-formation rate per comoving volume unit, the merger rate of binary BH-NS in triples is,

$$\Gamma_{\text{BH-NS}} = 8.1 \times 10^4 f_3 f_{\text{stable}} f_{\text{merge}} \text{ Gpc}^{-3} \text{ yr}^{-1}. \quad (13)$$

Here, f_3 is the fraction massive stars in triples, f_{stable} is the fraction of triple systems with an inner BH-NS binary that remain stable after the all the SN events take place,

and f_{merge} is the conditional probability that systems that are stable after all the SN events merge as a consequence of the KL mechanism. We adopt $f_3 = 0.15$ in our calculations. We find that the fraction of stable systems depends both on σ and on the progenitor metallicity, since lower Z 's produce more massive BHs, that on average receive lower kicks as a result of our assumption of momentum-conserving kicks. We find $f_{\text{stable}} \approx 1.4 \times 10^{-2}$, 1.8×10^{-5} , 2.6×10^{-7} for $\sigma = 0 \text{ km s}^{-1}$, 100 km s^{-1} , 260 km s^{-1} , respectively, when $a_{3,\text{max}} = 2000 \text{ AU}$ and $Z = 0.01$, and $f_{\text{stable}} \approx 5.5 \times 10^{-4}$, 1.4×10^{-4} , 1.6×10^{-6} , 2.6×10^{-7} , 5.1×10^{-8} , for $Z = 0.0001$, $Z = 0.001$, $Z = 0.005$, $Z = 0.01$, $Z = 0.015$, respectively, when $\sigma = 260 \text{ km s}^{-1}$ and $a_{3,\text{max}} = 2000 \text{ AU}$. In the case $a_{3,\text{max}} = 5000 \text{ AU}$, we find that the fraction of stable systems is about half of the case where $a_{3,\text{max}} = 2000 \text{ AU}$. Finally, we find that the typical fraction of systems that merge is $f_{\text{merge}} \sim 0.1$ (see Table 2). Plugging these numbers into Eq. 13,

$$\Gamma_{\text{BH-NS}} = 1.9 \times 10^{-4} - 22 \text{ Gpc}^{-3} \text{ yr}^{-1}. \quad (14)$$

Our estimate for the rate overlaps with BH-NS mergers in binaries (Kruckow et al. 2018) and is entirely within the LIGO allowed values (The LIGO Scientific Collaboration & the Virgo Collaboration 2018).

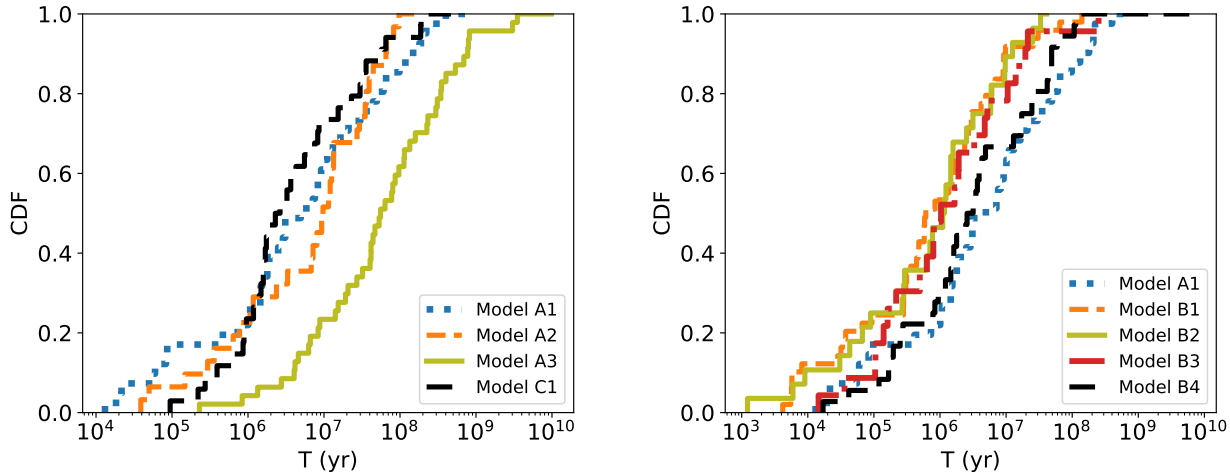


Figure 8. Merger time distribution (after the SN events) of BH-NS binaries in triples that lead to merger (see Table 2). Left panel: different values of σ and $a_{3,\max}$; right panel: different values of Z .

4 CONCLUSIONS

The possible recent detection of a BH-NS merger event by the LIGO-Virgo collaboration via GWs attracted much attention to these sources. BH-NS mergers are of high interest for their possible EM counterparts, such as short gamma-ray bursts, which can be observed by high-energy observatories and could provide crucial information on the related physics. While the formation of BH-NS binaries is not straightforward in star clusters as a result of the strong heating by BHs, isolated binary and triple systems can produce this type of mergers.

In this second paper of the series, we have followed-up our initial study (Fragione & Loeb 2019) of the dynamical evolution of triples comprised of an inner BH-NS binary. We have focused on how the progenitor metallicity affects the distributions of the relevant parameters of the BH-NS binaries that undergo a merger in triples. We have determined the distributions of BH masses, orbital parameters, and merger times as a function of the progenitor metallicity and initial triple orbital distributions, and derive a merger rate range of $\Gamma_{\text{BH-NS}} = 1.9 \times 10^{-4} - 22 \text{ Gpc}^{-3} \text{ yr}^{-1}$. Our range is in agreement with the rate derived from isolated binaries and the LIGO upper limit. The dependence of the BH masses, orbital parameters and rates on the metallicity could be tested by either identifying the host galaxy from EM counterpart or by detecting the evolution of the source properties with increasing redshift, thus decreasing metallicity on average.

We have also shown that the typical eccentricity of BH-NS binaries that merge in triple systems in the LIGO band is $\sim 10^{-2} - 10^{-1}$. Recent studies have shown that the orbital eccentricity is a useful tool for disentangling different production channels. Since GW emission is highly efficient at circularizing the orbit of an inspiraling BH binary, BHs that merge in isolation are expected to enter the LIGO frequency band (10 Hz) with very low eccentricities, $\sim 10^{-7} - 10^{-6}$. In case the BH binary merger is catalyzed by KL cycles in a hierarchical system, as in our case, a number of authors showed that the typical eccentricity distribution peaks at much higher values, $\sim 10^{-2} - 10^{-1}$, for various astrophysical

scenarios (Antonini et al. 2016; Fragione & Bromberg 2019; Fragione & Kocsis 2019; Fragione & Loeb 2019). The spectrum of eccentricities at LIGO band is much richer for BHs merging as a result of the dynamical assembly in a star cluster (Samsing et al. 2014b; Samsing & D’Orazio 2018). Zevin et al. (2018) demonstrated that there are three different possibilities in this scenario: (i) binaries that are ejected and merge outside the cluster have eccentricities $\sim 10^{-7} - 10^{-6}$, as in the isolated binary case; (ii) binaries that merge as a result of a GW capture process have eccentricities $\sim 10^{-2} - 10^{-1}$, as in the KL-induced mergers; (iii) binaries that merge within the cluster have intermediate eccentricities $\sim 10^{-5} - 10^{-3}$. In any case, matched-filtering searches for GWs do not utilize eccentric templates, thus no eccentric mergers have been observed so far by the LIGO-Virgo network.

BH and NS spin magnitudes can be a powerful observables to constrain the physics of massive stars. Spin magnitudes are expected to be set by the physics governing the stellar collapse, which can depend on the progenitor star metallicity and mass loss. How the specific properties of the progenitor set the properties of the remnant spin is still highly uncertain. Therefore, we have also investigated the expected spin-orbit misalignments of merging BH-NS binaries. In this channel, the spins of the BHs and NSs in the inner binary can undergo a relativistic precession around the inner angular momentum. Using a quadrupole approximation, Antonini et al. (2018) and Rodriguez & Antonini (2018) argued that BH binaries merging in a triple system would lead typically to near-zero effective spins. However, more recently, Liu et al. (2019) have showed by using a more accurate integration of the equations of motions that this is not the case and the effective spins are rather distributed more uniformly. We have found that typically the effective spin distribution is peaked at $\chi_{\text{eff}} \sim 0$, but with significant tails. Regarding other scenarios, binaries that evolve and merge in isolation are expected to have spin vectors that are relatively aligned with the angular momentum of the binary, thus having an effective spin always positive with $\cos \theta_{\text{BH}}, \cos \theta_{\text{NS}} \sim 1$ (Vitale et al. 2017; Gerosa et al. 2018). On the other hand, dynamically-assembled BHs in star clusters are expected to have spin vectors distributed isotropically with respect to

the orbital angular momentum, thus leading to a distribution peaked at $\chi_{\text{eff}} \sim 0$ with symmetric tails (Rodríguez et al. 2016; Arca Sedda & Benacquista 2019).

We note that in our simulations we check that the triples are stable after each SN event. However, systems that become unstable as a result of a SN may still produce a BH-NS merger, which we do not take into account in our results. We also note that we are assuming that the SNe take place instantaneously and do not simulate the systems during the main sequence lifetime of the progenitors. This and the details of the specific progenitor evolutions, which depend on winds, metallicity and rotation, could reduce the available parameter space for BH-NS mergers (see e.g. Shappee & Thompson 2013). The situation is even more complicated if mass loss during possible episodes of Roche-lobe overflows and common evolution phases in the triple are taken into account, which are not modeled as accurately as in binary systems (Di Stefano 2019; Hamers & Dosopoulou 2019). Mass transfer may likely harden the triple systems, possibly reducing the KL timescale thus the merger time. We also did not account for the fact that there could be an excess of systems with near-unity mass ratios and that the multiple fraction may be higher at low metallicities, if the triple were to follow the same trend of binaries (Moe & Di Stefano 2017; Moe et al. 2019). A near-unity mass ratio for the outer binary in our triples would imply a larger number of systems that remain bound after SNe take place, thus enhancing the merger rate of BH-NS binaries in triples.

The observation via GW emission of a merging BH-NS binary which enters the LIGO band with a high eccentricity and with a nearly zero effective spin would be a strong signature that the mechanism proposed in this paper is at work.

ACKNOWLEDGEMENTS

GF thanks Rosalba Perna and Raffaella Schneider for useful discussions on stellar evolution, and Johan Samsing for comments on an earlier version of the manuscript. GF thanks Seppo Mikkola for helpful discussions on the use of the code ARCHAIN. GF acknowledges support from a CIERA post-doctoral fellowship at Northwestern University. This work was also supported by the Black Hole Initiative at Harvard University, which is founded by a JTF grant (to AL).

REFERENCES

- Antonini F., Chatterjee S., Rodríguez C. L., Morscher M., Pattabiraman B., Kalogera V., Rasio F. A., 2016, *ApJ*, 816, 65
- Antonini F., Perets H. B., 2012, *ApJ*, 757, 27
- Antonini F., Rodríguez C. L., Petrovich C., Fischer C. L., 2018, *MNRAS*, 480, L58
- Antonini F., Toonen S., Hamers A. S., 2017, *ApJ*, 841, 77
- Arca Sedda M., Benacquista M., 2019, *MNRAS*, 482, 2991
- Arca-Sedda M., Li G., Kocsis B., 2018, arXiv e-prints, p. arXiv:1805.06458
- Arzoumanian Z., Chernoff D. F., Cordes J. M., 2002, *ApJ*, 568, 289
- Askar A., Szkudlarek M., Gondek-Rosińska D., Giersz M., Bulik T., 2017, *MNRAS*, 464, L36
- Banerjee S., 2018, *MNRAS*, 473, 909
- Bartos I., Kocsis B., Haiman Z., Márka S., 2017, *ApJ*, 835, 165
- Belczynski K., Holz D. E., Bulik T., O’Shaughnessy R., 2016, *Nature*, 534, 512
- Belczynski K., Klencki J., Meynet G., Fryer C. L., Brown D. A., Chruslinska M., Gladysz W., O’Shaughnessy R., Bulik T., Berti E., 2017, arXiv e-prints, p. arXiv:1706.07053
- Blaauw A., 1961, *Bulletin of the Astronomical Institutes of the Netherlands*, 15, 265
- Bothwell M. S., Kennicutt R. C., Johnson B. D., Wu Y., Lee J. C., Dale D., Engelbracht C., Calzetti D., Skillman E., 2011, *MNRAS*, 415, 1815
- de Mink S. E., Mandel I., 2016, *MNRAS*, 460, 3545
- Di Stefano R., 2019, arXiv e-prints, p. arXiv:1903.11618
- D’Orazio D. J., Levin J., 2013, *Phys. Rev. D*, 88, 064059
- Duchêne G., Kraus A., 2013, *Annual Review of Astronomy and Astrophysics*, 51, 269
- Eggleton P. P., 1983, *ApJ*, 268, 368
- Eldridge J. J., Stanway E. R., Tang P. N., 2019, *MNRAS*, 482, 870
- Foucart F., 2012, *Phys. Rev. D*, 86, 124007
- Fragione G., Bromberg O., 2019, arXiv e-prints, p. arXiv:1903.09659
- Fragione G., Grishin E., Leigh N. W. C., Perets H. B., Perna R., 2018, arXiv e-prints
- Fragione G., Kocsis B., 2018, *Phys Rev Lett*, 121, 161103
- Fragione G., Kocsis B., 2019, arXiv e-prints, p. arXiv:1903.03112
- Fragione G., Leigh N., Perna R., 2019, arXiv e-prints, p. arXiv:1903.09160
- Fragione G., Loeb A., 2019, *MNRAS*, 486, 4443
- Fragione G., Pavlík V., Banerjee S., 2018, *MNRAS*, 480, 4955
- Fryer C. L., Kalogera V., 2001, *ApJ*, 554, 548
- Gerosa D., Berti E., O’Shaughnessy R., Belczynski K., Kesden M., Wysocki D., Gladysz W., 2018, *Phys. Rev. D*, 98, 084036
- Gondán L., Kocsis B., 2019, *ApJ*, 871, 178
- Gondán L., Kocsis B., Raffai P., Frei Z., 2018, *ApJ*, 860, 5
- Grishin E., Perets H. B., Fragione G., 2018, *MNRAS*, 481, 4907
- Hamers A. S., Dosopoulou F., 2019, *ApJ*, 872, 119
- Hobbs G., Lorimer D. R., Lyne A. G., Kramer M., 2005, *MNRAS*, 360, 974
- Hurley J. R., Pols O. R., Tout C. A., 2000, *MNRAS*, 315, 543
- Iben Jr. I., 1991, *ApJS*, 76, 55
- Kobulnicky H. A., Kiminki D. C., Lundquist M. J., Burke J., Chapman J., Keller E., Lester K., Rolen E. K., Topel E., Bhattacharjee A., Smullen R. A., Vargas Álvarez C. A., Runnoe J. C., Dale D. A., Brotherton M. M., 2014, *The Astrophysical Journal Supplement Series*, 213, 34
- Kroupa P., 2001, *MNRAS*, 322, 231
- Kruckow M. U., Tauris T. M., Langer N., Kramer M., Izzard R. G., 2018, *MNRAS*, 481, 1908
- Liu B., Lai D., 2019, *MNRAS*, 483, 4060
- Liu B., Lai D., Wang Y.-H., 2019, arXiv e-prints, p. arXiv:1905.00427

- Maeder A., 2009, Physics, Formation and Evolution of Rotating Stars
- Mardling R. A., Aarseth S. J., 2001, MNRAS, 321, 398
- Marks M., Kroupa P., Dabringhausen J., Pawlowski M. S., 2012, MNRAS, 422, 2246
- Mikkola S., Merritt D., 2006, MNRAS, 372, 219
- Mikkola S., Merritt D., 2008, AJ, 135, 2398
- Moe M., Di Stefano R., 2017, ApJS, 230, 15
- Moe M., Kratter K. M., Badenes C., 2019, ApJ, 875, 61
- O’Leary R. M., Kocsis B., Loeb A., 2009, MNRAS, 395, 2127
- O’Leary R. M., Meiron Y., Kocsis B., 2016, ApJLett, 824, L12
- Pannarale F., Tonita A., Rezzolla L., 2011, ApJ, 727, 95
- Pijloo J. T., Caputo D. P., Portegies Zwart S. F., 2012, MNRAS, 424, 2914
- Podsiadlowski P., Langer N., Poelarends A. J. T., Rappaport S., Heger A., Pfahl E., 2004, ApJ, 612, 1044
- Rasskazov A., Kocsis B., 2019, arXiv e-prints, p. arXiv:1902.03242
- Rodriguez C. L., Amaro-Seoane P., Chatterjee S., Rasio F. A., 2018, PRL, 120, 151101
- Rodriguez C. L., Antonini F., 2018, ApJ, 863, 7
- Rodriguez C. L., Zevin M., Pankow C., Kalogera V., Rasio F. A., 2016, ApJ, 832, L2
- Samsing J., 2018, Phys. Rev. D, 97, 103014
- Samsing J., D’Orazio D. J., 2018, MNRAS, 481, 5445
- Samsing J., Hamers A. S., Tyles J. G., 2019, Phys. Rev. D, 100, 043010
- Samsing J., MacLeod M., Ramirez-Ruiz E., 2014a, ApJ, 784, 71
- Samsing J., MacLeod M., Ramirez-Ruiz E., 2014b, ApJ, 784, 71
- Sana H., 2017, in Eldridge J. J., Bray J. C., McClelland L. A. S., Xiao L., eds, The Lives and Death-Throes of Massive Stars Vol. 329 of IAU Symposium, The multiplicity of massive stars: a 2016 view. pp 110–117
- Sana H., et al., 2012, Science, 337, 444
- Sana H., Le Bouquin J. B., Lacour S., Berger J. P., Duvert G., Gauchet L., Norris B., Olofsson J., Pickel D., Zins G., Absil O., de Koter A., Kratter K., Schnurr O., Zinnecker H., 2014, The Astrophysical Journal Supplement Series, 215, 15
- Shappee B. J., Thompson T. A., 2013, ApJ, 766, 64
- Silber K., Tremaine S., 2017, ApJ, 836, 39
- Spera M., Mapelli M., Bressan A., 2015, MNRAS, 451, 4086
- The LIGO Scientific Collaboration the Virgo Collaboration 2018, arXiv e-prints, p. arXiv:1811.12907
- Toonen S., Hamers A., Portegies Zwart S., 2016, Computational Astrophysics and Cosmology, 3, 6
- Tsang D., Read J. S., Hinderer T., Piro A. L., Bondarescu R., 2012, Phys Rev Lett, 108, 011102
- Vitale S., Lynch R., Sturani R., Graff P., 2017, Classical and Quantum Gravity, 34, 03LT01
- Wen L., 2003, ApJ, 598, 419
- Ye C. S., Kremer K., Chatterjee S., Rodriguez C. L., Rasio F. A., 2019, arXiv e-prints, p. arXiv:1902.05963
- Zevin M., Samsing J., Rodriguez C., Haster C.-J., Ramirez-Ruiz E., 2018, arXiv:1810.00901